Pergamon

Ocean Engineering 27 (2000) 1199–1219

OCEAN ENGINEERING

Hydrodynamics of an oscillating water column seawater pump. Part II: tuning to monochromatic waves

S.P.R. Czitrom [a,*], R. Godoy [a], E. Prado [a], A. Olvera [b], C. Stern [c]

[a] *Instituto de Ciencias del Mar y Limnología, UNAM, Circuito Exterior S/N, Ciudad Universitaria, 04510 México D.F., Mexico*

[b] *Instituto de Investigación en Matemáticas Aplicadas y Sistemas, UNAM, Ciudad Universitaria, 04510 México D.F., Mexico*

[c] *Facultad de Ciencias, UNAM, Circuito Exterior S/N, Ciudad Universitaria, 04510 México D.F., Mexico*

Received 4 March 1999; accepted 7 May 1999

Abstract

Flume experiments with a scale-model of a wave driven seawater pump in monochromatic waves are described. A tuning mechanism optimises the pump performance by keeping it at resonance with the waves. The pumping process itself was found to de-tune the system because of the reduced gravity restoring force due to spilling in the compression chamber. A perturbation analysis of the pump equations shows that performance of the system can be increased by optimising the shape of the pump intake to minimise losses due to vortex formation. An algorithm is derived, using a numerical model of the pump, which accurately determines the required volume of air in the compression chamber to induce resonance given variations in the wave frequency, the wave height and the tides. A sustainable development project to use a seawater pump to manage fisheries at a coastal lagoon in Mexico is described.

Keywords: Waves; Pump; Resonance; Coastal management

* Corresponding author.
E-mail address: czitrom@mar.icmyl.unam.mx (S.P.R. Czitrom).

0029-8018/00/$ - see front matter
PII: S0029-8018(99)00041-4

1. Introduction

In Part I of this paper (Czitrom et al., 2000), a wave driven sea water pump, which has potential for various coastal management purposes such as aquaculture, flushing out of contaminated areas or the recovery of isolated coastal lagoons as breeding grounds, is described. Performance of the pump is optimised by a novel tuning mechanism, which allows it to resonate at various wave frequencies (Czitrom, 2000). An improved set of equations for the system was derived using the time dependent form of Bernoulli's equation and adding terms to account for viscous losses. The main improvement over the equations previously derived (Czitrom, 1997), is the realistic pressure loss term due to friction in laminar oscillating flow. A dimensional analysis of the pump equations shows that the proposed scale-model studied in this paper, functions similar to a full-scale system. The pump behaviour is basically linear and operates like a two mass-two spring system with relatively small non-linear losses (see Fig. 3 below). A basic tuning algorithm was derived, using the linearised pump equations, to estimate the volume of air required for resonance under varying wave and tidal conditions.

In this paper, the results from a series of wave tank tests with a scale-model of the pump are described. Performance of the pump is studied under various tuning conditions and an understanding of the processes that affect resonance is achieved. A numerical model, which integrates the pump equations, is used to derive a tuning algorithm for monochromatic waves. This algorithm provides an accurate estimate of the volume of air in the compression chamber required for resonance, given variations in the wave period, the wave height and the tidal elevation.

2. Experimental setup

A scale-model of the pump was built in acrylic plastic as shown in Fig. 1. The mouth of the resonant duct (A) was placed in the wave tank exposed to the passing waves, while the exhaust duct (C) was placed in a bucket of water (D), which was levelled flush with the surface of the tank. The pump was primed at the start of the experiments by creating a partial vacuum that brought water up from the tank and bucket, to the working level in the compression chamber (B). The volume of air in the compression chamber was modified by changing the level of water in the connecting chamber (E); through interchange with the storage tanks (F) beneath the pump. Dimensions of the various components can be obtained from Table 1 in Part I of this paper.

The wave-induced pressure signal at the mouth of the resonant duct drives an oscillating flow that spills water into the compression chamber, and through the exhaust duct to the bucket of water, with each passing wave. Air in the chamber behaves like a spring against which water in the resonant and exhaust ducts oscillates. Maximum efficiency is attained at resonance when the system natural frequency of oscillation coincides with the frequency of the driving waves (see Lighthill, 1979; Evans, 1982; Falnes and McIver, 1985). A resonant condition can be maintained for

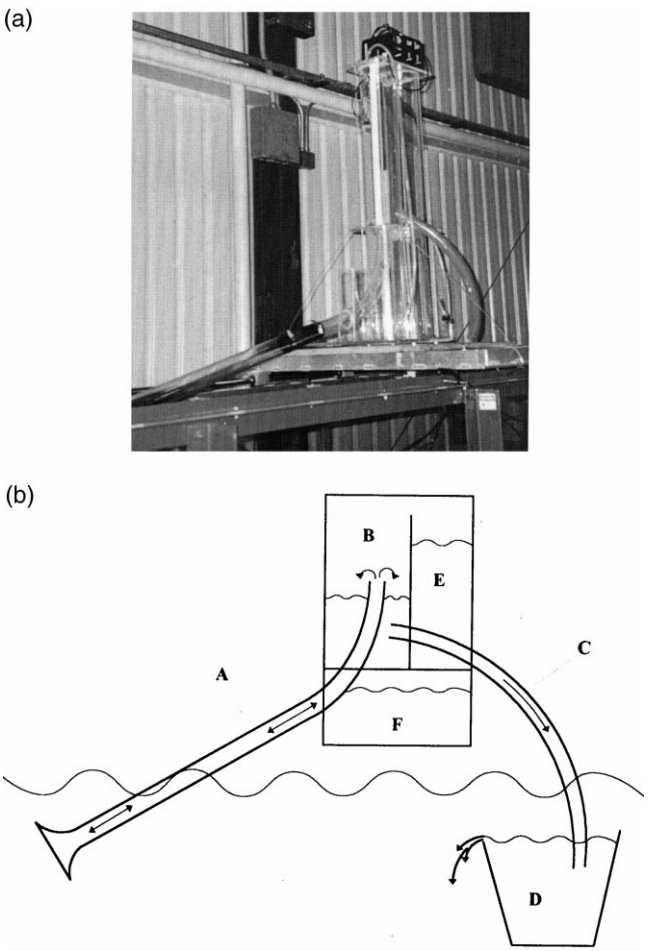

Fig. 1. Model of the wave energy driven sea-water pump. The resonant (A) and exhaust (C) ducts had 0.056 and 0.036 m diameters respectively while the compression chamber had a diameter of 0.145 m. Resonant and exhaust duct lengths were 4.08 and 15 m. The equilibrium level in the compression chamber was placed 1.26 m above te wave tank surface.

different wave frequencies by means of the variable volume compression chamber that adjusts the hardness of the air spring.

The pump was fully instrumented with water height sensors of the capacitance type in the resonant and exhaust ducts, at the compression chamber, and piezoelectric pressure sensors at the duct mouth and in the compression chamber. An additional water height sensor was placed near the resonant duct mouth to monitor the driving wave height. Flow rate through the pump was measured by timing the water spilt at the bucket with a calibrated vessel. In the water height sensors, an insulated wire and the surrounding grounded water make up the two poles of a capacitor, which are separated by the insulator thickness. Capacitance of the sensor changes with the

length of wire submerged, which in turn modifies the frequency of an electronic oscillator. Comparison to a stable high frequency signal (2 MHz) yields a voltage that changes linearly with the water height. Sensitivity was 1 mV/mm within a range of 0 to 350 mV±0.5 mV. The pressure transducers had a high integrity silicon diaphragm with a titanium module of sensitivity 2 mV/PSI in a range 0–100 mV±1%. The signals were digitised to an 11 bit accuracy.

During the experiments, the wave period and its profile were modified using the tank control computer, to give sinusoidal wave trains as well as polychromatic wave packets. Results shown in this paper correspond to sinusoidal wave trains of 2.25 s period and 0.05 m amplitude. Performance of the pump was monitored for various tuning conditions by changing the volume of air in the connecting compression chamber. The effect on pump performance of the resonant duct sill height in the compression chamber was also tested.

3. The numerical model

$$(X_1+L_1(1+\varepsilon_1)+T_d/\cos\theta)\ddot{X}_1+\frac{\dot{X}_1^2}{2}+\left(\frac{K_1}{2}+\frac{(L_1+T_d/\cos\theta)}{D_1}f_1+C_{r1}\right)\dot{X}_1|\dot{X}_1| + \frac{(P_A-\rho gH)}{\rho}\left[\left(1-\frac{A_1X_1}{V_o}-\frac{A_cX_2}{V_o}\right)^{-\gamma}-1\right]+g\cdot\cos\theta\cdot X_1=W/\rho, \tag{1a}$$

$$\left(X_2+\frac{A_c}{A_2}L_2(1+\varepsilon_2)+L_c\right)\ddot{X}_2+\frac{\dot{X}_2^2}{2}+\left(\frac{K_2}{2}+\frac{L_2}{D_2}f_2+C_{r2}\right)\left(\frac{A_c}{A_2}\right)^2\dot{X}_2|\dot{X}_2| + \frac{(P_A-\rho gH)}{\rho}\left[\left(1-\frac{A_1X_1}{V_o}-\frac{A_cX_2}{V_o}\right)^{-\gamma}-1\right]+gX_2=0. \tag{1b}$$

A numerical model of the pump was written in Turbo Pascal for an IBM compatible PC to simulate water surface displacement in the resonant and exhaust ducts. Eqs. (1a) and (1b) for the non-pumping half of the cycle and (9) of Part I of this paper, which apply when there is spilling in the compression chamber, were integrated forward in time using a simple finite difference forward integration scheme. This scheme delivered indistinguishable results from the Runge–Kutta method of integration but has the advantage of greater speed and flexibility during the spilling stage at the resonant duct sill. The numerical model was driven by the observed pressure signal at the duct mouth. For a full derivation of the pump equations and a description of the frictional pressure losses in oscillating flow (the terms with f_i) see Part I of this paper.

Subscripts 1, 2 and c in Eqs. (1a) and (1b) correspond to the resonant and exhaust ducts and compression chamber respectively. X is the surface displacement, in either duct, relative to its equilibrium position in the compression chamber, and L, D and A are lengths, diameters and areas respectively. L_1 (the resonant duct length) and T_d (the tidal height) are referred to the equilibrium position on the exhaust duct side of the compression chamber. In addition:

P_A atmospheric pressure (kg m^{-1} s^{-2})
ρ sea water density (kg m^{-3})
$\gamma = C_p/C_v$ air compressibility=1.4
W wave pressure signal (kg m^{-1} s^{-2})
T_d Height of sea level above receiving body of water (includes tidal signal) (m)
V_o compression chamber volume (m^3)
H height of compression chamber equilibrium position above receiving body of water (m)
ε fractional added length due to edge effects at the duct mouth
θ resonant duct inclination at the compression chamber
$g' = g\cos\theta$ Reduced gravity due to inclination of the resonant duct at the compression chamber (m s^{-2})
f friction loss coefficient for oscillating flow in pipes
K vortex formation energy loss coefficient (see Knott and Mackley, 1980)
C_r radiation damping coefficient (see Knott and Flower, 1980).

Fig. 2 shows a plot of water height in the resonant and exhaust ducts as well as the driving pressure signal against time, for one of the experiments. Both numerical model and observations are plotted here. It can be seen that the model reproduces observations remarkably well despite some discrepancy at the spilling stage when the sill is overtaken by water in the resonant duct. Splashing in the compression

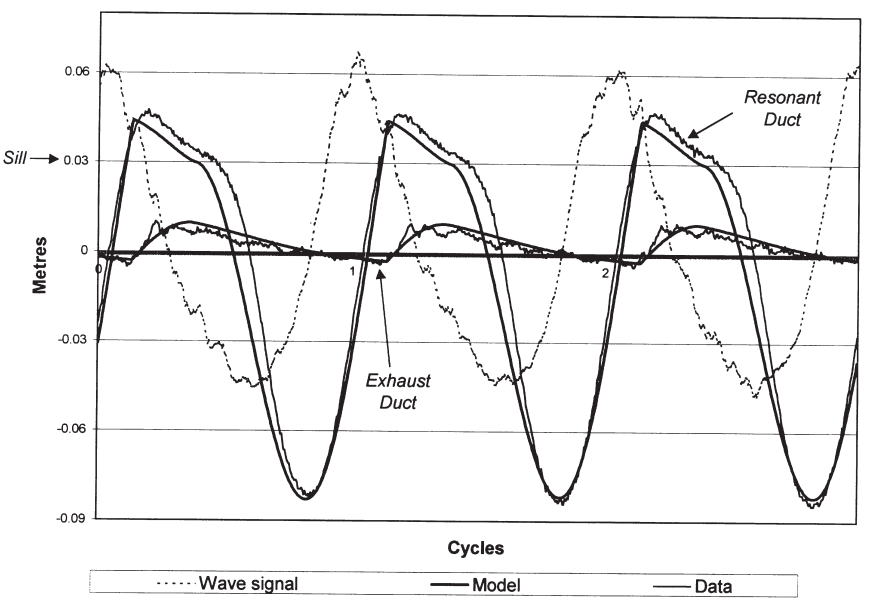

Fig. 2. Modelled and observed resonant and exhaust duct water heights at the compression chamber and driving wave height plotted against time. Wave period was 2.25 s and resonant duct sill height 0.03 m.

chamber during spilling appears as high frequency oscillations in the exhaust duct measurement trace.

Integrating the pump equations requires defining values for the coefficients ε, K and C_r. ε, the proportion by which the duct lengths are increased by edge effects at the duct-mouths (otherwise known as added mass), is easily determined by requiring that the modelled and observed maximum values in Fig. 3 coincide. Here flow through the pump is plotted against the volume of air in the compression chamber (the hardness of the air spring), so that variations in ε modify the volume of air at which resonance occurs; that is, the position of the maximum in the numerical model values along the abscissa. This procedure gave an ε of 0.06, that is, a 6% added mass due to edge effects at the mouths.

The coefficients $K/2+C_r$ in equations (1), for losses due to vortex formation at the mouth and radiation damping in the resonant and exhaust ducts, were adjusted to obtain the best fit between the numerical model and the observed data. These coefficients were adjusted as a unit since they are not distinguishable with the data acquired. Adjustments were made using plots like that shown in Fig. 2, as well as the observed and modelled flow through the pump (Fig. 3). Increasing or decreasing these coefficients affects the size of the modelled predictions in these figures. In the case of the resonant duct, values were adjusted for the upward ($K_1/2+C_r=3.5$), and

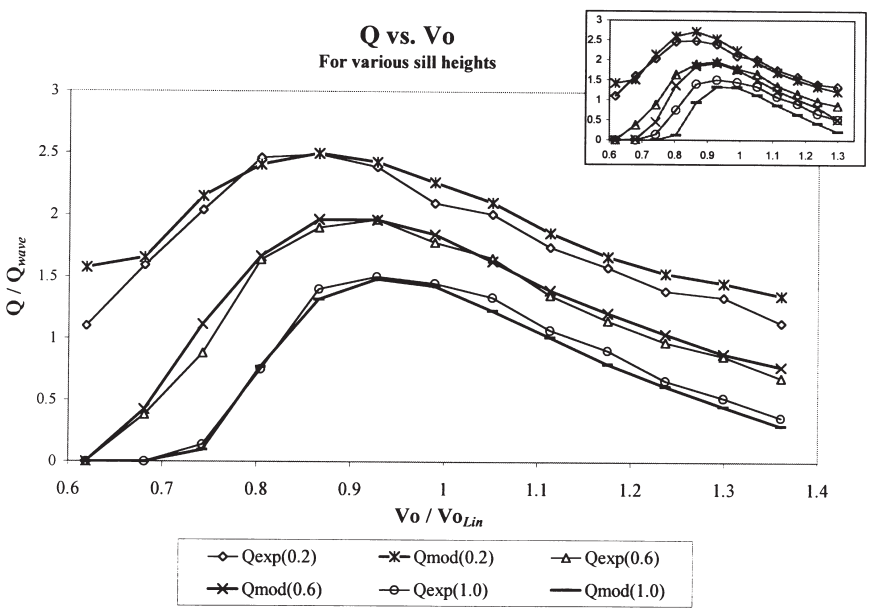

Fig. 3. Observed (Q_{exp}) and modelled flow (Q_{mod}) through the pump against compression chamber air volume for the three resonant duct sill heights (above the water level in the compression chamber). Flow is scaled with $Q_{wave}(=A_1a/T)$, the volume of water in a section of resonant duct one wave amplitude long, per wave period. The ordinate is scaled with the volume of air required for resonance in the linearised model (2) and the sill height is scaled with the wave amplitude. The insert at the upper right hand corner is a similar plot presented by Czitrom (1997).

the downward ($K_2/2+C_r=5$) strokes. The lower loss coefficient for the upward stroke in the resonant duct appears to reflect a more orderly flow on entry, due to the presence of a trumpet shaped funnel which was placed at the duct mouth, than on exit. For experiments without the circular profile funnel, the required upward stroke coefficient increased to 4, and flow through the pump was ~10% lower than that shown in Fig. 3. It appears that the funnel increases performance of the pump by diminishing vortex losses at the duct mouth (see also Knott and Flower, 1980 and Fig. 5). A unique value of $K/2+C_r=5$ was required for the exhaust duct since, as flow oscillates back and forth, fluid enters on one side of the duct and exits on the other so that there is no preferred direction.

Fig. 3 shows much improved numerical model predictions of flow than a similar plot presented by Czitrom (1997) (reproduced at the upper right hand corner). This is partly the result of having used a more appropriate friction loss term in the pump equations, as already noted, but also of having used the measured pressure signal at the duct mouth to drive the numerical model, rather than the depth attenuated water height signal used previously. Fig. 4 shows FFT analyses of the pressure signal measured at the duct mouth (divided by ρg) and of the water surface height measured above the pressure sensor. It can be seen that the amplitude of the main frequency of the pressure signal is actually *greater*, by a factor of 1.1, than that of the surface signal, while the reverse occurs with the first harmonic. Normally the wave induced pressure signal becomes attenuated with depth according to a well-known relation; which in our case gives a value of 0.85. It appears that the presence of the duct mouth increases the size of the pressure signal relative to that of the unperturbed

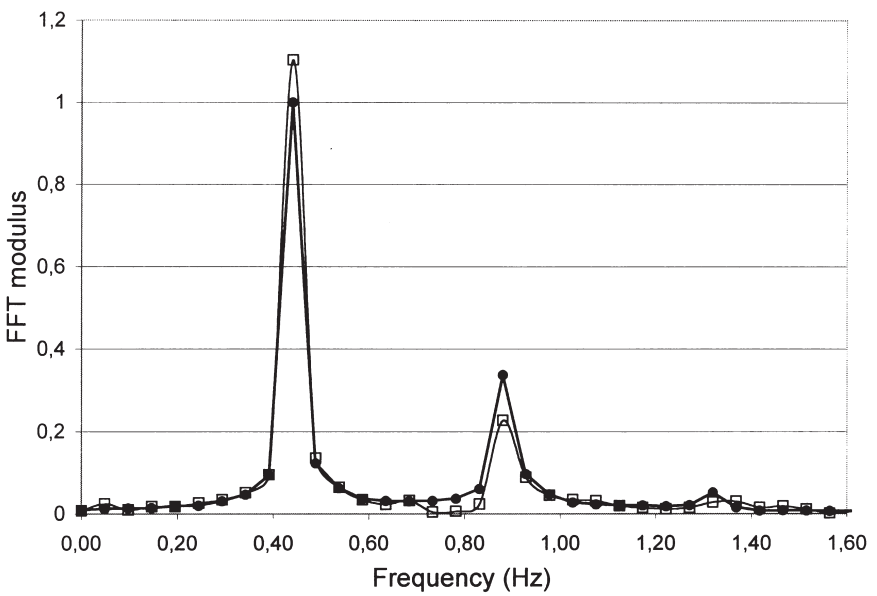

Fig. 4. Fast Fourier Transforms of the water height signal above the resonant duct mouth (heavy line) and of the pressure signal measured at the entrance (divided by ρg).

wave at the intake by a factor of 1.3. When the duct entrance was not fit with the funnel shaped mouth, amplification of the pressure signal by the presence of the duct was reduced to 1.15. This result is similar to that found by Lighthill (1979), although under very different circumstances, and is currently being further investigated. It seems that this effect will improve performance of the pump.

It was noted earlier that flow through the pump increased by 10% when the mouth of the resonant duct was fitted with a trumpet shaped mouth. Preliminary experiments, presently being carried out, in effect show a far more complex and wide ranging vortex field, representing greater energy losses, when the funnel shaped mouth is not present (see Fig. 5). Various trumpet profile designs will be tested in the new experiments, in an attempt to optimise performance of the pump. The relation between the enhanced wave induced pressure signal at the duct mouth and vortex losses is also being further explored.

The numerical model predictions in Figs. 2 and 3 were obtained using the above values for the added mass, vortex and radiation loss coefficients throughout. The excellent fit to the data indicates that, referring to relations (2) and (4) of Part I of this paper, the loss coefficients K and C_r are not very sensitive to changes in the Reynolds, modified Reynolds and Strouhal numbers, within the ranges covered in these experiments. Further work remains to be carried out to cover wider experimental conditions, such as those encountered in oceanic conditions.

4. Tuning the wave driven pump

While operating the pump, a resonant condition can be achieved by adjusting the natural frequency of oscillation of the system, increasing or decreasing the volume of air in the compression chamber, so that it coincides with the frequency of the driving waves. Performance of the pump is optimal at resonance since the system absorbs energy from the waves at peak efficiency and fluid oscillations in the ducts are maximised.

It was shown in Part I of this paper that, in the absence of spilling in the compression chamber, the wave driven seawater pump can be represented by two masses, two springs and two non-linear dampers coupled as shown in Fig. 6. The spring on the left represents gravity in the resonant duct, L_1 and L_2 represent the resonant and exhaust duct masses, respectively, and the spring in the middle represents the air compression chamber. The pistons represent the non-linear losses due to friction, vortex formation and radiation damping in the resonant and exhaust ducts. It was also shown that the linear terms dominate the system behaviour with the non-linear terms making only small contributions.

Neglecting the non-linear terms in equations (1), it was shown that a first approximation to the volume of air required for resonance is given by:

$$V_{oLin}=\frac{(P_A-\rho gH)\gamma}{\rho}\left[\frac{A_1}{L_1'\Omega^2-g'}+\frac{A_c}{L_2'\Omega^2}\right]. \tag{2}$$

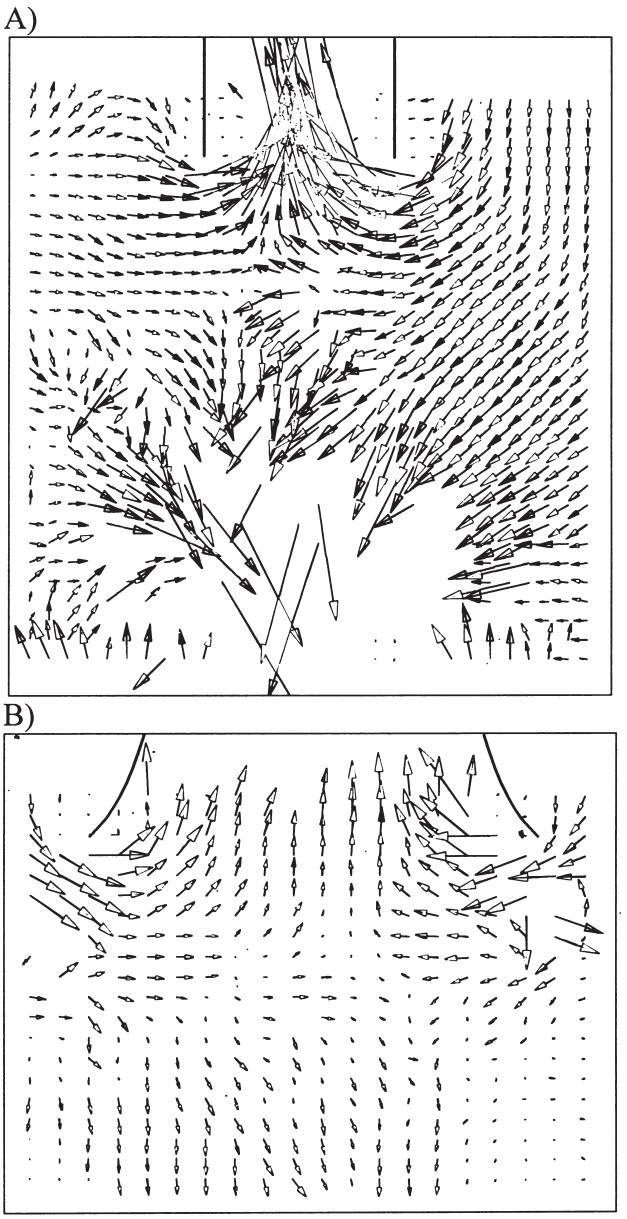

Fig. 5. Exit flow vectors obtained: (A) without and (B) with a trumpet shaped funnel at the resonant duct mouth. Vectors were obtained with a laser particle visualisation system for Re=4×10^3 and Re*m*=10^3.

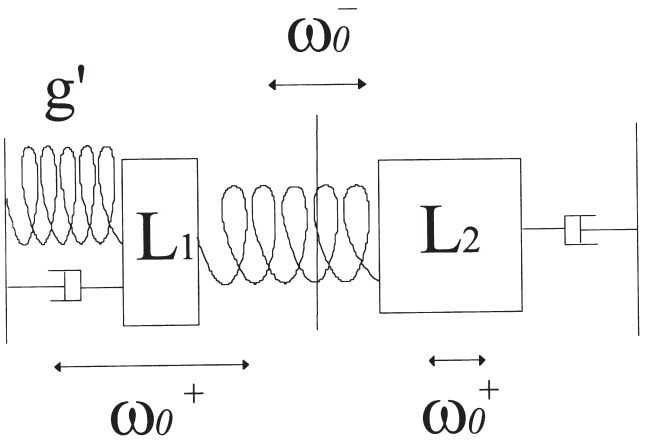

Fig. 6. Representation of the model pump as a damped, two mass, spring oscillator.

This algorithm is as good as the friction, vortex formation and radiation damping losses are small relative to the linear terms retained. A further limitation is that it does not take into account the pumping process itself since it was derived using only equations (1) which apply when there is no spilling in the compression chamber.

Expression (2) was used to scale the tuning air volume in Fig. 3, where flow data for the model pump are shown plotted against the compression chamber volume, for three sill heights. Also shown are flow values from the numerical integration of the pump equations. It can be seen that the shape of the curves and the tuning air volume for which maximum pumping occurs are reproduced remarkably well by the numerical model. Greater flow is obtained for smaller sill heights because fluid in the resonant duct runs a shorter distance before spilling occurs. It can also be seen that as the sill height diminishes (and flow increases), the optimal air volume in the compression chamber becomes increasingly smaller than the resonant volume for the linear model (1 on the horizontal scale). Keeping the pump tuned to this volume represents a loss in flow of at least 10% for the smallest sill height, and it is thus worth while finding a better tuning algorithm that can account for the observed shift.

We now address the shift towards smaller resonant air volumes with decreasing sill height in Fig. 3. Czitrom et al. (1996) proposed that this shift might be ascribed to the increase in resonant duct length at smaller sill heights and to a de-tuning effect of the non-linear terms in equations (1). While the increase in length is a contributing factor, it can be shown that it is not large enough to account for all the observed shift. We now first explore the de-tuning effect of the friction and other non-linear terms in the pump equations, and then the processes that occur during pumping.

In order to study the de-tuning effect of the non-linear terms, we will use the non-dimensional version of equations (1a) and (1b), scaled with the wave period and amplitude, as given by equations (3a) and (3b) (for a full description of the non-dimensional equations see Part I of this paper).

$$\Lambda_1\ddot{\chi}_1+\frac{A_{f1}}{2}\dot{\chi}_1^2+\left(\frac{K_1}{2}+C_{r1}+\frac{L_1}{D_1}f_1\right)A_{f1}\dot{\chi}_1|\dot{\chi}_1|+K\left[\left(\chi_1+\frac{L_1}{L_2}\chi_2\right)+K'\left(\chi_1+\frac{L_1}{L_2}\chi_2\right)^2\right.$$
$$\left.+K''\left(\chi_1+\frac{L_1}{L_2}\chi_2\right)^2+\ldots\right]+\Gamma_1\chi_1=\Delta\cos(\tau), \tag{3a}$$

$$\Lambda_2\ddot{\chi}_2+Z_1^2\frac{A_{f1}}{2}\dot{\chi}_2^2+\left(\frac{K_2}{2}+C_{r2}+\frac{L_2}{D_2}f_2\right)Z_2^2A_{f1}\dot{\chi}_2|\dot{\chi}_2|+K\left[\left(\chi_1+\frac{L_1}{L_2}\chi_2\right)\right.$$
$$\left.+K'\left(\chi_1+\frac{L_1}{L_2}\chi_2\right)^2+K''\left(\chi_1+\frac{L_1}{L_2}\chi_2\right)^3+\ldots\right]+\Gamma_2\chi_2=0. \tag{3b}$$

Here

$$\Lambda_1=\left(\frac{L_1(1+\varepsilon)}{a}+\frac{T_d}{a\cos\theta}\right),\ \Lambda_2=\frac{L_1(1+\varepsilon)}{a}\frac{A_1}{A_2},\ K=\frac{(P_A-\rho gH)\gamma A_1}{\rho a\Omega^2V_o},\ K'=\frac{(\gamma+1)aA_1A_{f1}}{2V_o},$$
$$K''=\frac{(\gamma+1)(\gamma+2)a^2A_1^2A_{f1}^2}{6V_o^2},\ \Gamma_1=\frac{g\cos\theta}{a\Omega^2},\ \Gamma_2=\frac{g}{a\Omega^2}\frac{L_1A_1}{L_2A_c},\ Z_1=\frac{L_1A_1}{L_2A_c},$$
$$Z_2=\frac{L_1A_1}{L_2A_2},$$

and

$$\Delta=\frac{g}{a\Omega^2A_{f1}}.$$

It can be seen that, since $L_2\gg L_1$ in the laboratory conditions and χ_1 and χ_2 are of order 1, the effect of the exhaust duct on the compression chamber term (fourth in equations (3)), which couples both equations, is small. It is thus reasonable to decouple both equations by making $\chi_2=0$ and work only with the resonant duct equation. This equation can thus be rewritten as:

$$\ddot{\chi}+\omega_0^2\chi+\lambda(\eta\chi^2+\zeta\chi^3+\mu\dot{\chi}|\dot{\chi}|+\xi\dot{\chi}+\varsigma\dot{\chi}^2)=\lambda F\cos\tau. \tag{4}$$

Parameter λ has been introduced in Eq. (4) as a scale for the terms that are small when compared to the acceleration $\ddot{\chi}$, as well as for the external forcing, to analyse the equation using perturbation methods. The components of Eq. (4) can be identified as follows: $\ddot{\chi}$ is the acceleration and $\omega_0^2=(\Gamma_1+K)/\Lambda_1$ is the square of the natural frequency of oscillation (normalised with the driving wave frequency Ω) due to the restitution force from gravity and the linear part of the compression chamber. $\eta=KK'/\Lambda_1$ and $\zeta=KK''/\Lambda_1$ come from the quadratic and cubic non-linear restitution force from the compression chamber respectively. $\mu=(K/2+C_r)/\Lambda_1$ results from vortexes and radiation damping and $\xi=\Sigma_1\Sigma_1'/\Lambda_1$ and $\varsigma=\Sigma_1/2\Lambda_1$ come from the linear and the first non-linear components of the friction term for the laboratory, respectively. $F=\Delta/\Lambda_1$ is the term due to the forcing wave.

We chose a Krylov & Bogoliubov averaging method (Nayfeh, 1973) to obtain the solution to order λ. Starting with the linear solution (λ=0) given by $\chi_0=\beta\cos(\omega_0 t+\delta)$, we can consider that β and δ, when λ is no longer zero, will be functions of time which change very slowly, such that if we define a new time scale λt, then β and δ are functions of this scale. By means of the averaging method we can obtain the differential equations for the amplitude and phase functions:

$$\langle\dot{\beta}\rangle=\lambda\left(-\frac{4\mu\omega_0\beta^2}{3\pi}-\frac{1}{2}\xi\beta+\frac{F}{2\omega_0}\sin(\psi)\right), \tag{5a}$$

$$\beta\langle\dot{\psi}\rangle=\lambda\left(\beta\sigma-\frac{3}{8}\frac{\zeta\beta^3}{\omega_0}-\frac{F}{2\omega_0}\cos(\psi)\right), \tag{5b}$$

where $\psi=\sigma\lambda t-\delta$ and $\lambda\sigma=\Omega-\omega_0$. Here we focus our interest on the analysis close to resonance by setting the difference between the forcing frequency and the system natural frequency to order λ and defining σ as the de-tuning. We can trace the effect of each perturbation term in Eq. (4) into the equations for the amplitude and phase. The first term in Eq. (5a) corresponds to vortex formation and radiation damping, the middle term is due to the linear part of the friction loss and the last term in both equations (5a and b) comes from the external forcing. The second term in Eq. (5b) corresponds to the cubic non-linear term of the compression chamber. The constant and quadratic parts of the friction loss and the quadratic term from the compression chamber do not contribute to either the amplitude or the phase at order λ.

To find the asymptotic behaviour of Eq. (5a) we consider the situation in which β and ψ have reached their steady state value, i.e. $\langle\dot{\beta}\rangle=\langle\dot{\psi}\rangle=0$. From the resulting expressions the dependence of the amplitude β on the external forcing amplitude F can be examined. Taking only the vortex formation and radiation damping term into account, β is proportional to $F^{1/2}$, while the contributions of the linear part of the friction loss and the cubic non-linear term of the compression chamber are proportional to F and $F^{1/3}$, respectively.

Adding the quadratic form of equations (5a) and (5b), the terms which depend on ψ can be eliminated. The asymptotic expression for β is then reduced to:

$$\frac{9}{64}\frac{\zeta^2}{\omega_0^2}\beta^6+\left(\frac{16}{9\pi^2}\mu^2\omega_0^2-\frac{3}{4}\frac{\zeta\sigma}{\omega_0}\right)\beta^4+\frac{4}{3\pi}\mu\omega_0\xi\beta^3+\left(\sigma^2-\frac{1}{4}\xi^2\right)\beta^2-\frac{F^2}{4\omega_0^2}=0 \tag{5c}$$

Close to resonance, that is when $|\sigma|\ll 1$, we are interested in finding the response amplitude β in terms of the external force F. Using the values shown in Table 2 of Part I of this paper and the fact that σ is very small, only the second and last terms are retained in Eq. (5c). For the resonant period used in our experimental set-up (T=2.25 s), the following asymptotic expression for the amplitude β is obtained:

$$\hat{\beta}\cong 0.31\sqrt{F}$$

Numerical experiments carried out with the non-pumping stage equations show that

the amplitude of the oscillations in the resonant duct are proportional to the square root of the forcing wave amplitude. A regression between the amplitude of the oscillation in the resonant duct and a, for the numerical model at resonance, yields $0.73\ a^{0.4986}$ with an R^2 of 0.99998. This result shows that the asymptotic solution provides the same functional form as the numerical model. We can therefore conclude that, in the laboratory conditions, vortex formation and radiation damping represent the main perturbation and that they control the amplitude of the oscillatory response within the device and therefore also the amount of flow that is pumped in the resonance regime. This conclusion corroborates the usefulness of improving the design of the resonant duct mouth to minimise losses due to vortex formation, in order to increase flow through the pump.

We now analyse Eq. (5b) in order to find a quantitative estimate of the de-tuning phenomenon. Let us suppose that the amplitude β has reached its asymptotic value $\hat{\beta}$. Also, we set the shift parameter $\sigma=0$ and the forcing term $F=0$. The solution of Eq. (5b) is then linear in time, and therefore the effective frequency is now

$$\omega_0-\frac{3}{8}\frac{\zeta}{\omega_0}\hat{\beta}^3,$$

showing that the actual frequency depends on the amplitude β. The resonant frequency shift from the unperturbed value ω_0 is a function of the amplitude, and can be expressed as:

$$\hat{\sigma}=\frac{3\zeta}{8\omega_0}\hat{\beta}^2$$

Using the values for the parameters shown in Table 2 of Part I of this paper and the asymptotic value for $\hat{\beta}$, we estimate $\hat{\sigma}\approx 10^{-5}F$. If we define V_o^* as the new resonant volume, $(V_{o\mathrm{Lin}}-V_o^*)/V_{o\mathrm{Lin}}$ is order 10^{-4} which is indistinguishable from the linear prediction for the resonant volume. We thus conclude that the pressure loss terms due to friction, vortex formation and radiation damping, cannot account for the shift observed in Fig. 3.

We now turn to the pumping process itself as a means of explaining the observed shift in the resonant air volume. In the simplified linear model of the pump described with Fig. 6, the restoring force for the fluid in the resonant duct is provided by a combination of the air compression and the gravity springs. During pumping, the fluid that spills from the resonant duct ceases to weigh on the rest of the fluid in that duct so that the gravity restoring force becomes constant. This is felt by the resonant duct as a softening of the restoring force since springiness is now only provided by the compression chamber. Pumping thus decreases the natural frequency of oscillation of the system so that, in order to maintain a resonant condition at the driving wave frequency, the compression chamber spring must be hardened, by decreasing its volume. This mechanism explains why maximum pumping occurs nearer the linear resonant volume for large sill heights (when pumping occurs during a small portion of the cycle), and becomes increasingly shifted towards smaller volumes as the sill height diminishes and pumping increases.

A crude estimate of the shift in the resonant volume due to this effect can be

made if we assume that the gravity spring restoring force in the resonant duct becomes negligible during half of the cycle (for low sill heights). If we simulate this effect with an overall gravitational acceleration of $g'/2$ for the resonant duct, V_o/V_{oLin} becomes, to a first approximation:

$$1-\frac{g'}{2L_1'(\Omega^2-g'/L_1')\left[1+\frac{A_cL_1'}{A_1L_2'}\left(1-\frac{g'}{L_1'\Omega^2}\right)\right]}, \tag{6}$$

using Eq. (2). Substituting values for the experimental conditions, the above expression gives 0.81, which is certainly large enough to explain the observed shift (~0.87). It thus appears that the softened-spring mechanism, due to pumping, is responsible for the shift in the natural frequency of oscillation observed in Fig. 3.

5. Obtaining an adequate tuning algorithm

A more adequate tuning algorithm, which includes the effect of spilling, requires finding solutions to equations (1) for the non-pumping stage and coupling them to the solutions of equations (9 of Part I of this paper) for the spilling stage. Considering the various non-linearities present, this is most likely an unfeasible task. We alternatively resort to the numerical model of the pump, which has already been shown to solve the system equations successfully, to obtain the required algorithm.

The appropriate algorithm must cater for variations in wave frequency, wave height, tidal elevation and sill height. That the driving wave period affects the resonant air volume needs no further comment. That the wave height also affects tuning can be understood by considering that larger waves must result in greater pumping and, as we have already seen, the pumping process significantly influences tuning. Tidal elevation on the other hand affects tuning by changing the water column length in the resonant duct, thus altering its mass. Finally, it can be seen in Fig. 4 that tuning is significantly influenced by the sill height as it increases or decreases flow through the pump.

A series of numerical model runs were performed to obtain the optimal resonant air chamber volume for various wave periods (1.5–3 s), wave heights (0.01–0.1 m), tidal elevations (0 to −0.09 m) and sill heights (0–0.025 m); for a pump configuration of the model experiments. For each set of T, a and T_d values (wave period, wave amplitude and tidal elevation respectively), the maximum (or resonant) flow through the pump was obtained by sweeping through a range of air chamber volumes and sill heights. The corresponding air volumes for resonance were fit to a Taylor series expansion to the fourth order in three dimensions:

$$V_o(T,a,T_d)=\sum_{k=0}^{4}\frac{1}{K!}\left[((T,a,T_d)-(T_0,a_0,T_{d0}))\cdot\left(\frac{\partial}{\partial T},\frac{\partial}{\partial a},\frac{\partial}{\partial T_d}\right)\right]^k V_o(T_0,a_0,T_{d0}) \tag{7}$$

by multiple regression. Here T_0, a_0 and T_{d0} are intermediate wave period, wave ampli-

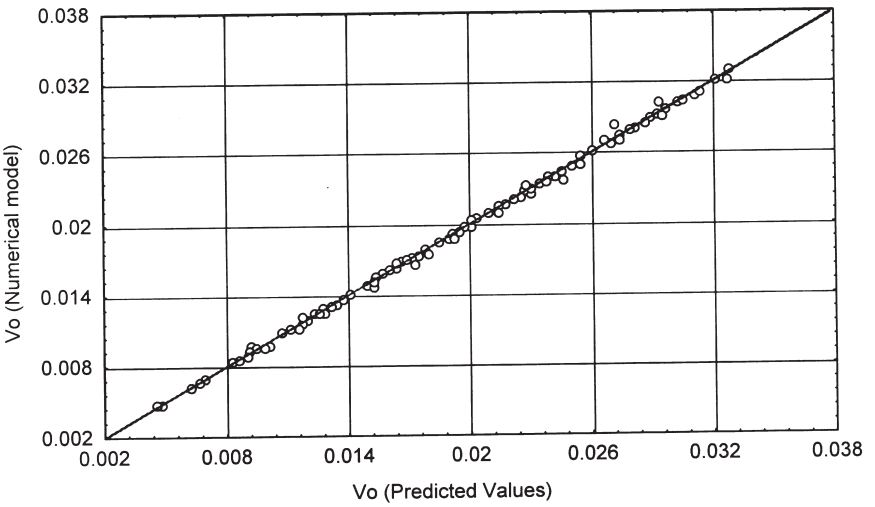

Fig. 7. Predicted (multiple regression) vs observed (numerical model results) resonant air chamber volumes for the 253 T, a, and T_d data sets.

tude and tidal elevations respectively. Values for the partial derivatives in the previous equation were estimated in the regression, giving the influence of each variable to the fourth power and the various interactions. Similar Taylor expansions were used in regressions for the optimum sill height $S_o(T,a,T_d)$ and resonant flow through the pump $Q_o(T,a,T_d)$. The regressions were performed on 253 data sets using the STATISTICA package which gives an estimate of each terms' significance in explaining the variance. Only the most significant terms were retained.

A plot of resonant volumes, obtained with the numerical model, against those predicted by the multiple regression equation, can be seen in Fig. 7. Complementing this plot, Table 1 shows the % of variance explained for the V_o, S_o and Q_o regression equations as well as the standard deviation of the observations about the predictions for all 253 data sets. It is apparent that a fourth order Taylor expansion gives a good approximation to the required resonant air chamber volumes, optimal sill heights and resonant flow.

The regression equations for V_o and S_o provide algorithms for adjusting the pump air volume and sill height for optimal resonant flow through the pump given a wave

Table 1
Percent of variance explained and standard deviations about the predictions for the V_o, S_o and Q_o regressions

Dependent variable	% of variance explained (R^2)	Standard error of estimate
V_o (m^3)	99.91	0.00023 m^3
S_o (m)	95.67	0.00103 m
Q_o (m^3 s^{-1})	99.05	0.0000045 m^3 s^{-1}

period, a wave height and a tidal elevation. The regression equation for Q_o provides an algorithm with which flow through the pump at resonance can be estimated for these values. These algorithms can be used with confidence for T, a, and T_d values within the limits used in the numerical model runs described above. Outside these ranges, the predictions deteriorate rapidly.

The experimental values depicted in Fig. 3 were obtained for a period of 2.25 s, a wave amplitude of 0.05 m and a tidal elevation of 0 m. Substituting in the regression equation for $V_o(T, a, T_d)$, and dividing by the linear resonant volume (from Eq. (2)), an optimal resonant volume of 0.865 is obtained. This compares very favourably with the observed optimal resonant volume of ~0.87 in Fig. 3. The standard error of the prediction (0.00023 m^3) represents a 0.017 variation in the horizontal scale of Fig. 3, confirming that the method described for obtaining the tuning algorithm is quite satisfactory.

For the same T, a, and T_d values, the regressions for S_o and Q_o estimate the optimal sill height at 0.163 and the flow through the pump at resonance at 2.31 (scaled with the same factors as in Fig. 3). From Fig. 3 it can be seen that the observed resonant flow through the pump is somewhat greater than this value. This is because a depth attenuated sinusoidal wave was used to drive the numerical model for the regressions, while the observed pressure signal was used for Fig. 3. This is further evidence that the presence of the resonant duct mouth enhances the pressure signal with respect to the unperturbed depth attenuated wave.

V_o and Q_o are best visualised in the 3D plots shown in Figs. 8 and 9 where data points and spline interpolation surfaces are presented. In Fig. 8a, the air chamber volume needed for resonance (V_o m^3) is plotted against the wave periods (T s) and the tidal elevations (T_d m) covered in the numerical simulations described above. In Fig. 8b, V_o is plotted against the wave amplitudes (a m) and the tides.

It can be seen in Fig. 8a that, for increasing wave periods, greater air chamber volumes are required for the pump to resonate. Referring to Fig. 6, this is quite logical since a softer middle spring (greater air chamber volume) is required to diminish the natural frequency of oscillation for resonance to occur at a larger forcing period. It can also be seen in Fig. 8a that the resonant air chamber volume increases with diminishing tidal height. This is because the length, and therefore mass, of the resonant duct diminishes as the tides fall, which in turn increases the natural frequency of oscillation of the system in Fig. 6. In order to maintain resonance at the driving wave period, this increase in frequency must be compensated for by a softer middle spring (greater air chamber volume) to diminish the natural frequency of oscillation.

In Fig. 8b, at low tides, the resonant volume decreases with increasing wave amplitude. This can be explained by considering that the proportion of the cycle spent pumping also must increase with wave size, since the water surface equilibrium position in the resonant duct is well below the sill. Thus, an increase in wave size diminishes the effective gravity, which in turn requires a smaller volume of air to maintain resonance. In the absence of tides, however, the resonant volume *increases* with the wave amplitude. In this case the proportion of the cycle spent pumping will not change substantially because the equilibrium position in the resonant duct is near

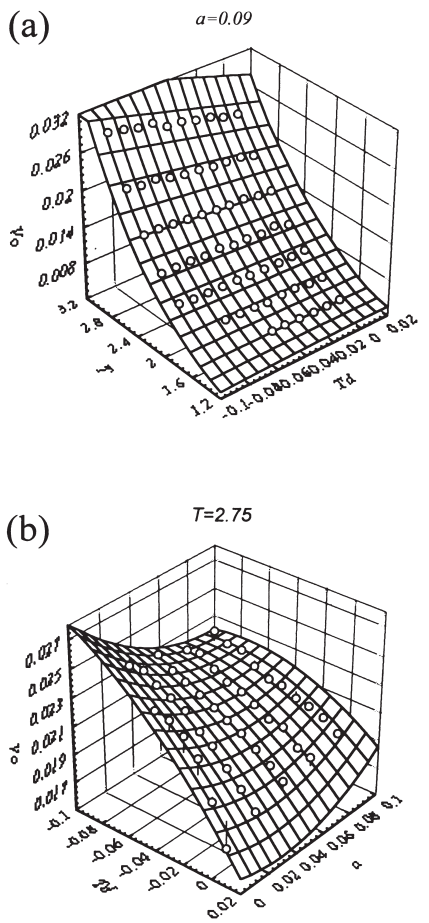

Fig. 8. Resonant air chamber volume (V_o) plotted (a) against the wave period and the tidal height (constant wave amplitude a=0.09 m) and (b) against the wave amplitude and the tidal height (constant wave period T=2.75 s).

the sill. The increase in volume is likely the result of an interplay with the sill optimisation, not directly interpretable in terms of the model in Fig. 6.

Observing the ranges in Fig. 8 it can be seen that, for the T, a, and T_d values covered in the numerical simulations, the resonant air volume is affected, in decreasing order of importance, by the wave period, the tidal height and the wave amplitude.

Similar to Fig. 8, Fig. 9a and b show flow through the pump at resonance (Q, m^3 s^{-1}) for the T, a, T_d and sill values swept in the numerical simulations. From Fig. 9a it is clear that flow increases with increasing wave period and increasing wave amplitude. That flow should intensify with increasing wave amplitude needs no further comment, except that, according to the perturbation analysis, the increase in flow is curbed to a $a^{1/2}$ shape by vortex and radiation losses. The raise in flow with

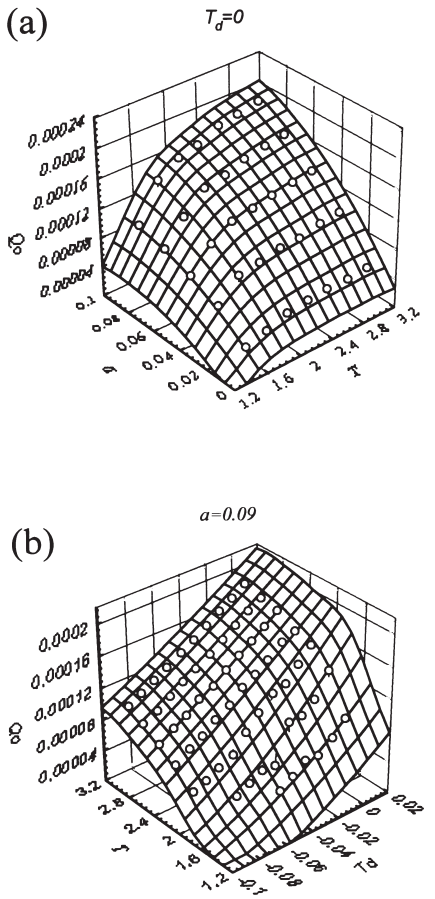

Fig. 9. Resonant flow through the pump (Q_o) plotted (a) against wave period and wave amplitude (constant tidal height T_d=0 m) and (b) against wave period and tidal height (constant wave amplitude a=0.09 m).

increasing wave period is reasonable considering that, at resonance, greater fluid oscillations can be expected at larger periods.

In Fig. 9b it can be seen that flow through the pump diminishes as the tide decreases. As the tide falls, the equilibrium surface level in the resonant duct drops and water in the resonant duct must run a longer distance before surpassing the resonant duct sill so that spilling occurs during a smaller proportion of the oscillation cycle. For small wave periods and large tides, water in the resonant duct can no longer surpass the sill and pumping ceases. It can be seen in Fig. 9 that, for the T, a, and T_d ranges covered in the simulations, flow through the pump is affected more or less equally by the wave period, the wave height and the tidal elevation.

6. Conclusions and final remarks

In this paper, a wave driven seawater pump, which has potential for various coastal management purposes such as aquaculture, flushing out of contaminated areas or the recovery of isolated coastal lagoons as breeding grounds, is studied. Performance of the system is optimised by a novel tuning mechanism, which allows it to resonate at various wave frequencies. The system was studied using a wave-tank model and numerical integrations of the pump equations. Performance of the numerical model improved significantly by using a new form for the friction loss term, and by taking into account the effect of the resonant duct mouth on the wave induced pressure field.

The reduced gravity restoring force on the resonant duct, during spilling in the compression chamber, was shown to cause a de-tuning with respect to the linear model of the pump. A method was developed to obtain a tuning algorithm, which takes this effect into account, using the numerical model. Tuning was shown to be a useful method for increasing performance of the pump under varying wave frequency, wave height and tide conditions which would otherwise fall by a considerable percentage. In the laboratory case described, it was found that tuning is sensitive, in decreasing order, to changes in the driving wave period, tidal height and wave height. Flow through the pump raises with increasing wave period, decreasing tide and increasing wave amplitude, all three contributing significantly.

A perturbation analysis of the non-linear terms in the pump equations showed that the vortex losses at the resonant duct mouth contribute significantly to limiting flow through the pump. Further work must be carried out to optimise the mouth design, in order to inhibit vortex formation in oscillatory flow. Various mouth designs are being tested to identify the most adequate design. Not enough is known about frictional losses in fully turbulent oscillatory flow in ducts. In order to improve the numerical models for oceanic conditions, further work must be carried out to obtain a more appropriate algorithm for pressure losses in such flow. A further problem to approach is the enhanced pressure fluctuations due to the presence of the duct mouth in a wave field.

The tuning procedure described in this paper was developed for monochromatic wave trains. Under realistic sea conditions, however, waves at a particular place are a composite of several frequencies and amplitudes; monochromatic waves being a fairly uncommon occurrence. From Fig. 3 it can be inferred that the sea water pump responds to a range of frequencies with varying efficiencies. Criteria are being developed to tune the system for optimal performance when driven by waves with observed power spectra. Alternatively, work is being carried out to develop a pump design based on parametric resonance, to take advantage of the relative insensitivity of this type of resonance on the driving frequency. Also, amplification in parametric resonance is exponential with time rather than linear so that efficiency might be significantly increased.

Wave energy conversion devices that operate by resonance are designed to perform optimally at fixed, average wave climate conditions. Performance is increased when out of resonance by implementing phase control mechanisms. The work described in this paper shows that a tuning mechanism, based on a variable volume air com-

pression chamber, could be a useful alternative device for increasing performance of OWC power systems.

With the help of a co-operative of village fishermen, a small experimental prototype of the wave driven pump was installed briefly during 1995 on the coast of Oaxaca, Mexico, to show that it could be used to manage the fisheries of a coastal lagoon. Since the pump has no moving parts, larvae of fish and shrimp pass undamaged through the system to fertilise, in a controlled manner, a lagoon that is increasingly cut off from the Pacific Ocean by littoral sediment transport. Working on a low budget (<US$10,000), the system was installed by hand, pulling the floating resonant duct through the surf zone with cables that passed through pulleys anchored at sea. The system successfully pumped larvae over the sand bar to the lagoon for a few days, at a rate compatible with the numerical model predictions. Unfortunately, after a fortnight, waves from a tropical storm ripped away the resonant duct entrance and the prototype had to be taken away. The fishermen were quite satisfied with the tests and at present we are working to install a full-scale permanent system at their lagoon. Special care is being taken to make the system robust to heavy weather, especially after a hurricane devastated the area in October 1997. Parallel to the pump installation, a multidisciplinary project is being carried out with the support of the MacArthur Foundation and the North American Fund for Environmental Co-operation. The biological and chemical components of the project will provide information to manage the lagoon's fisheries, taking care not to damage the ecosystem. Social aspects are also being addressed to promote a positive impact of the project on the local community. Environmental education programmes with the village children and work with various local grass roots organisations will hopefully result in the community appropriation of the project and in the promotion of sustainable development in the region. Other uses envisioned for the wave driven seawater pump described in this paper include the flushing out of contaminated marine areas or coastal lagoons.

Acknowledgements

We wish to thank the John D. and Catherine T. MacArthur Foundation, through a grant from the Fund for Leadership Development, for their generous support in carrying out the work presented in this paper. Support was also provided by the Dirección General de Apoyo al Personal Académico (Projects IN-104193, 106694 and 107197) and the Instituto de Ciencias del Mar y Limnología (Project "Energía de Oleaje" No. 139), both from the National University of Mexico (UNAM). Support was also provided by CONACyT through project "Matemáticas no-lineales en la Física y en la Ingeniería," No. 625427-E. We wish to thank Prof. Tony Dalrymple, Joe Hammack, Nobu Kobayashi and Brad Johnson for allowing and helping us to use the wave tanks at the Center for Applied Coastal Research, The University of Delaware. Thanks are also due to Ranulfo Rodríguez Sobreyra for developing and implementing the sensing and data acquisition system used during the experimental work.

References

Czitrom, S.P.R., 1997. Wave energy-driven resonant sea-water pump. Journal of Offshore Mechanics and Arctic Engineering, Transactions of the ASME 119, 191–195.

Czitrom, S.P.R., 2000. Patent pending. Sintonizador para sistemas de extraccion de energía de oleaje que operan por resonancia. Solicitud de Patente Mexicana No. 933605.

Czitrom, S.P.R., Godoy, R., Prado, E., Pérez, P., Peralta-Fabi, R., 2000. Hydrodynamics of an oscillating water column seawater pump. Part I: theoretical aspects. Ocean Engineering 27, 1181–1198.

Czitrom, S.P.R., Prado, E., Godoy, R., Rodríguez, R., Peralta, R., 1996. Sea-water pumping by resonance II. In: Proceedings of the Second European Wave Power Conference, Lisbon, November. pp. 324–328.

Evans, D.V., 1982. Wave-power absorption by systems of oscillating surface pressure distributions. Journal of Fluid Mechanics 114, 481–499.

Falnes, J., McIver, P., 1985. Surface wave interactions with systems of oscillating bodies and pressure distributions. Applied Ocean Research 7 (4), 225–234.

Knott, G.F., Flower, J.O., 1980. Measurement of energy losses in oscillatory flow through a pipe exit. Applied Ocean Research 2 (4), 155–164.

Knott, G.F., Mackley, M.R., 1980. Eddy-motions near plates and ducts induced by water waves and periodic flows. Philosophical Transactions of the Royal Society 294A (1412), 599–623.

Lighthill, J., 1979. Two-dimensional analyses related to wave-energy extraction by submerged resonant ducts. Journal of Fluid Mechanics 91 (2), 253–317.

Nayfeh, A., 1973. Perturbation methods. Wiley, New York, 228–307.